ELSEVIER

NDT&E International, Vol. 30, No. 6, pp. 359–370, 1997

Printed in Great Britain
PII: S0963-8695(97)00005-4
0963-8695/97 $17.00+0.00

Performance of iterative tomographic algorithms applied to non-destructive evaluation with limited data

P. M. V. Subbarao, P. Munshi*, K. Muralidhar

Department of Mechanical Engineering, Indian Institute of Technology, Kanpur 208 016, India

Received 28 August 1996; accepted 21 December 1996

Iterative tomographic algorithms have been applied to the reconstruction of a two-dimensional object with internal defects from its projections. Nine distinct algorithms with varying numbers of projections and projection angles have been considered. Each projection of the solid object is interpreted as a path integral of the light-sensitive property of the object in the appropriate direction. The integrals are evaluated numerically and are assumed to represent exact data. Errors in reconstruction are defined as the statistics of difference between original and reconstructed objects and are used to compare one algorithm with respect to another. The algorithms used in this work can be classified broadly into three groups, namely the additive algebraic reconstruction technique (ART), the multiplicative algebraic reconstruction technique (MART) and the maximization reconstruction technique (MRT). Additive ART shows a systematic convergence with respect to the number of projections and the value of the relaxation parameter. MART algorithms produce less error at convergence compared to additive ART but converge only at small values of the relaxation parameter. The MRT algorithm shows an intermediate performance when compared to ART and MART. An increasing noise level in the projection data increases the error in the reconstructed field. The maximum and RMS errors are highest in ART and lowest in MART for given projection data. Increasing noise levels in the projection data decrease the convergence rates. For all algorithms, a 20% noise level is seen as an upper limit, beyond which the reconstructed field is barely recognizable.

Keywords: absorption, tomography, iterative algorithms, convergence rates, sensitivity to noise, errors

Introduction

There is continuing interest in the application of radiation techniques in non-destructive testing and inspection of many industrial products, namely composite materials, steel slabs produced by continuous casting and other processes, lumber processing, nuclear reactor cores, integrated circuits and printed circuit boards. Developments in computer-aided image acquisition and image processing have led to accelerated usage of these methods. Progress in two- or three-dimensional reconstruction, tomographic techniques has permitted the generation of complete objects using the radiation data as one- or two-dimensional projections.

Image reconstruction from projections can be viewed as a linear inverse problem with discrete data. Exact inversion has been commonly carried out in the past using the convolution backprojection algorithm. This algorithm requires projection data for a large number of angles and the projection data must be equal to the field to be reconstructed. In many problems it may not be possible to

* Correspondence to Prof. P. Munshi

acquire such a large amount of projection data. With limited data, one encounters an ill-posed problem in reconstruction of a field from an incomplete set of projections. Several iterative techniques have been proposed to address such problems. In the present work, three groups of iterative algorithms namely the algebraic reconstruction technique (ART), the multiplicative algebraic reconstruction technique (MART) and the maximization reconstruction technique (MRT) have been considered. They have been applied to the reconstruction of two-dimensional fields. Specifically, a cosGauss phantom has been employed for explicit determination of errors. This is followed by an application to a circular region with circular holes. The performance of the three sets of algorithms has been evaluated in terms of convergence rates, residual error and sensitivity to noise in the projection data.

Reconstruction methods based on series expansions made their first appearance in the scientific literature and in the computerized tomography (CT) scanner industry around 1970. ART is an example and is frequently used[1]. All algorithms that fall into the ART family are classified into two major groups, namely additive ART and multiplicative ART (MART). These algorithms are further classified into sub-groups based on how different parts of the algorithms are implemented. The major steps of an ART algorithm are the integration procedure to obtain approximate projections, the calculation of weighting functions, the structure of correction terms and the procedures used to correct the field value.

As in the conventional ART method, additive or multiplicative corrections are possible in all the algorithms which belong into the ART family. Recent studies have indicated that, of the several classes of reconstruction algorithms applicable for limited data, those based on the multiplicative algebraic reconstruction technique (MART) are the fastest, most flexible and accurate. Verhoeven[2] presented various types of MART algorithms and suggested modifications for the reconstruction of multidirectional interferometric data. However all the algorithms suggested by the author require low relaxation parameters.

As limited-data tomography does not have a unique solution, the reconstruction equations may be viewed as the equality constraints for maximization (or minimization) of a function such as entropy or energy. The problem of reconstruction using limited data will have an infinite number of solutions. This shows that one has to obtain an optimal solution out of these many solutions. The MENT algorithm produces a solution with maximum entropy to the problem of reconstruction. From the standpoint of information theory this approach is conceptually attractive: it yields the image with the lowest information content consistent with the available data[3,4]. Gull and Newton[5] have described other possible functions besides entropy which can be extremized to obtain reconstructed data. Herman[6] reconstructed the head phantom using MENT. Myers and Hanson[7] compared the performance of ART and MENT in the reconstruction of a source object with 10 high-contrast and 10 low-contrast discs. Reis and Roberty[8] reconstructed solid objects with complex internal features using a limited number of projections.

Absorption tomography

Tomography is the process of recovery of a 'function' from a set of its integrals along well-defined directions called 'hyperplanes'[9]. In absorption methods, the attenuation of the intensity of radiation traversing a transparent fluid or solid is measured. Consider the application of tomography with absorption. The local field here is taken as the coefficient of absorption $\mu(x, y, z)$. The generally applicable Lambert–Beer absorption law can be written as

$$I = I_0 e^{-\mu s} \tag{1}$$

The integral measurement is the attenuation of the intensity of radiation $I(r, \theta)/I_0$ which is related to the absorption coefficient as

$$\ln\left(\frac{I(r,\theta)}{I_0}\right) = \int_s \mu(x, y, z)\, \mathrm{d}s \equiv p \tag{2}$$

where I_0 is the initial intensity of the radiation at the entrance into the investigated volume and I is the local intensity dependent upon the absorption coefficients μ and s. It is possible to generate the complete two-dimensional field using projections of μ defined by Equation (2). In general, reconstruction is performed by using as many integral measurements as possible.

The absorption technique produces one-dimensional images containing information regarding the average intensity of the radiation. The absorption coefficient is, apart from being a function of the physical properties of the substance, also a function of the wavelength of radiation. For this reason, monochromatic waves, namely X-rays or τ-rays, are used in absorption measurements and suitable corrections are employed when X-rays (polyenergetic) are used. The images can be viewed as projections of the absorption coefficient field through Equation (2). The absorption coefficient field is recovered by inverting Equation (2) using the central slice theorem[10] as

$$\mu(r, \theta) = \int_{-\infty}^{\infty} \int_{-\infty}^{\infty} \left[\int_{-\infty}^{\infty} p e^{-i2\pi rS}\, \mathrm{d}r \right] e^{i2\pi(xX + zZ)}\, \mathrm{d}X\, \mathrm{d}Z \tag{3}$$

Explicit reconstruction methods that employ Equation (3) use the convolution-back projection algorithm[11]. Analytical methods show that errors in reconstruction are small only if a large number of views and a large number of rays per view are employed and a proper choice of parameters is made[12]. If this requirement is difficult to fulfil, iterative techniques discussed in the present study show the potential for reconstruction with a limited number of views.

The iterative reconstruction methods are based on the discretization of the cross-sectional plane by a square grid

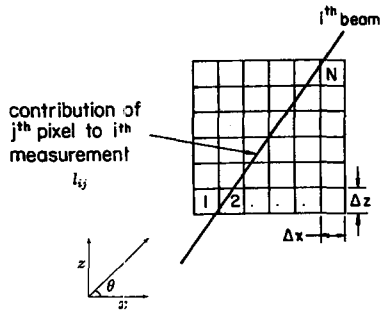

Figure 1 Definition of a weighting function

(Figure 1). The length of the intercept of a ray with the jth cell in a given projection is called the weight function. In construction of fields with a large number of grids, a weight of 1 if a ray passes through a cell and 0 otherwise is used. A more accurate procedure is to calculate weights (Figure 1) as

$$w_{i,j} = \frac{l_{ij}}{\sqrt{(dx^2 + dz^2)}} \tag{4}$$

If f_j is the field value in the jth cell, the ith projection is given as

$$\phi_i = \sum_{j=1}^{N} w_{ij} f_j \quad i = 1, 2, ..., M \tag{5}$$

This discretization produces a matrix equation

$$[w_{ij}]\{f_i\} = \{\phi_i\} \tag{6}$$

The problem of tomographic reconstruction thus reduces to inversion of this matrix. Iterative techniques can be thought of as a solution of Equation (6) through a generalized inverse of matrix $[w_{ij}]$.

Series expansion methods

Series expansion methods are iterative and consist necessarily of four major steps: assumption of the test field, calculation of correction, application of correction and test for convergence. These algorithms differ in the manner in which corrections are applied and presented in brief below (for details, see Subbarao and Muralidhar[13]).

Simple ART

Mayinger[14] has suggested the simplest possible iterative reconstruction algorithm which in many ways resembles the algebraic reconstruction algorithm. Let $\phi_{i\theta}$ be the projection due to the i_θth ray with angle of irradiation θ and $\tilde{f}_i$ be the initial guess of the field value, We compute the approximation projection $\tilde{\phi}_{i_\theta}$ using the test field as

$$\tilde{\phi}_{i_\theta} = \sum_{j=1}^{N} w_{i_\theta,j} f_j \quad i_\theta = 1, 2, ..., M_\theta \tag{7}$$

where i_θ denotes the ith ray of an irradiation with angle θ, and $1 \leq i_\theta \leq M_\theta$. The subsequent steps are as follows.

- For each angle of radiation θ

(1) For each ray i_θ calculate the correction $\Delta\phi_{i_\theta} = \phi_{i_\theta} - \tilde{\phi}_{i_\theta}$
(2) Compute the total value of the weight function along each ray as $W_{i_\theta} = \sum_{j=i}^{N} w_{i_\theta,j}$
(3) Calculate the average value of correction

$$\overline{\Delta\phi_{i_\theta}} = \frac{\Delta\phi_{i_\theta}}{W_{i_\theta}}$$

(4) Repeat Steps 1–3 for all rays.
(5) Apply a correction for each cell j of the test field as

$$\tilde{f}_j^{\,\text{new}} = \tilde{f}_j^{\,\text{old}} + \lambda\overline{\Delta\phi_{i_\theta}}$$

where λ is the relaxation factor.
(6) Repeat Step 5 for all the rays of the irradiation with angle θ.

- Update the approximate projection using Equation (7).
- Repeat the above procedure for all angles of irradiation. This completes the kth global iteration.
- Iterate until

$$\frac{f^{k+1} - f^k}{f^k} \times 100 \leq e$$

where e is the stopping criterion, say 0.01%.

Gordon ART

The ART algorithm originally proposed for CT applications by Gordon *et al.*[1] is considered. In this method corrections are applied to all the cells through which the ith ray passes, before calculating the correction for next ray. Hence the number of rays per angle of irradiation is not important. As in Equation (5), the approximate projection data is computed as

$$\tilde{\phi}_i = \sum_{j=1}^{N} w_{ij} f_j \quad i = 1, 2..., M \tag{8}$$

where M is the grand total number of rays and N is the number of cells. The remaining part of the algorithm can be stated as follows.

- For each iteration k

(1) For each ray i calculate the correction $\Delta\phi_i = \phi_i - \tilde{\phi}_i$
(2) Compute the correction coefficient $\alpha_i = \sum_{J=1}^{N} w_{ij}^2$
(3) Apply a correction to each cell j of the test field through which the present ray passes as

$$\tilde{f}_j^{\,\text{new}} = \tilde{f}_j^{\,\text{old}} + \lambda\frac{w_{ij}\Delta\phi_i}{\alpha_i}$$

(4) Repeat Steps 1–3 for all the rays.

This completes the kth iteration.

- Iterate until

$$\frac{f^{k+1}-f^k}{f^k}\times 100 \le e$$

- Calculate again the approximate projection using Equation (8) and iterate until the stopping rule is satisfied.

Gilbert ART

Gilbert[15] has developed independently a form of an ART, called the simultaneous iterative reconstruction technique (SIRT). In SIRT, the elements of the field function are modified after all the correction values corresponding to individual rays have been calculated. The algorithm is similar to ART but the correction is applied as given below.

- For each iteration k

(1) For each ray i calculate the correction $\Delta\phi_i = \phi_i - \tilde{\phi}_i$
(2) Compute the correction coefficient $\alpha_i = \sum_{j=i}^{N} w_{ij}^2$
(3) Repeat Steps 1 and 2 to all the rays.

- Identify all the rays (Nc_j) passing through a given cell and the corresponding w_{ij} and $\Delta\phi_i$.
- For each cell j apply the algebraic sum of all possible correction terms as

$$\tilde{f}_j^{\,\text{new}} = \tilde{f}_j^{\,\text{old}} + \sum_{ic=1}^{Nc_j} \lambda \frac{w_{ij}\Delta\phi_i}{\alpha_i}$$

This completes the kth iteration.

- Iterate until

$$\frac{f^{k+1}-f^k}{f^k}\times 100 \le e$$

- Calculate a new value of the approximate projection using Equation (8) until the stopping criterion is satisfied.

Anderson ART

Anderson and Kak[16] has proposed a new algorithm, simultaneous ART (SART) which combines the ART and SIRT algorithms. It was found to be very efficient and superior in implementation. The method of applying a correction is similar to simple ART but the structure is similar to ART. The algorithm is as follows.

- For each angle of radiation θ

(1) For each ray i_θ calculate the correction $\Delta\phi_{i_\theta} = \phi_{i_\theta} - \tilde{\phi}_{i_\theta}$
(2) Compute the correction coefficient $\alpha_{i_\theta} = \sum_{j=i}^{N} w_{i\theta,j}^2$
(3) Repeat steps 1–2 for all rays belong to irradiation with angle θ.
(4) Apply a correction to each cell j of the test field as

$$\tilde{f}_j^{\,\text{new}} = \tilde{f}_j^{\,\text{old}} + \lambda \frac{w_{i_\theta j}\Delta\phi_{i_\theta}}{\alpha_{i\theta}}$$

Here λ is the relaxation factor.

(5) Repeat Step 4 to all rays of the irradiation with angle θ.

- Calculate the new value of the approximate projection using Equation (7).
- Repeat the above procedure to all angles of irradiation. This complete the kth global iteration.
- Iterate until

$$\frac{f^{k+1}-f^k}{f^k}\times 100 \le e$$

- Continue iterations until the stopping rule is satisfied.

Multiplicative ART

The correction strategies presented in above are called additive ART (or simply ART). When the correction is multiplicative, the ART is called multiplicative ART (MART). In the present work, MART with three different types of correction formulae have been implemented. The initial approximate projection is computed using Equation (8). The MART algorithms considered in the present study are as follows.

- For each iteration k

(1) For each ray i calculate the approximate projection $\tilde{\phi}_i$
(2) Identify all the rays passing through a given cell (the total number of rays per cell being Nc_j) and corresponding i, w_{ij}, ϕ_i and $\tilde{\phi}_i$
(3) For each cell j compute the product of all possible correction terms. This can be accomplished in three different ways as

$$MART1: \quad \tilde{f}_j^{\,\text{new}} = \tilde{f}_j^{\,\text{old}} \times \prod_{Nc_j}\left[1-\lambda\left(1-\frac{\phi_i}{\tilde{\phi}_i}\right)\right]$$

$$MART2: \quad \tilde{f}_j^{\,\text{new}} = \tilde{f}_j^{\,\text{old}} \times \prod_{Nc_j}\left[1-\lambda w_{ij}\left(1-\frac{\phi_i}{\tilde{\phi}_i}\right)\right]$$

$$MART3: \quad \tilde{f}_j^{\,\text{new}} = \tilde{f}_j^{\,\text{old}} \times \prod_{Nc_j}\left[\frac{\phi_i}{\tilde{\phi}_i}\right]^{\lambda w_{ij}}$$

This completes the kth iteration.

- Iterate until

$$E \equiv \frac{f^{k+1}-f^k}{f^k}\times 100 \le e$$

- Update the approximate projection using Equation (8)
- Continue iterations until $E \le e$.

Maximum entropy

Maximum entropy techniques (MENT) have been receiving increasing attention in the literature on image processing. They produce an unbiased solution and are maximally non-committal about unmeasured parameters[5]. This algorithm is outlined below.

Consider a continuous function $f(x, y, z)$ which satisfies the condition

$$f(x, y, z) \ge 0$$

Then, entropy optimization refers to the mathematical problem of maximizing the functional

$$F(x,y,z) = -\iiint f(x,y,x)\ln[f(x,y,z)]\,dz\,dy\,dx \qquad (9)$$

over various sets of constraints.

If f_j is the discrete form of $f(x,y,z)$, then Equation (9) can be rewritten as

$$F_j = -\sum_{j=1}^{n} f_j \ln[f_j] \qquad (10)$$

In image reconstruction the collected data and any other *a priori* information comprise the constraints over which entropy is maximized. A typical problem would be

$$\text{maximise}\left(-\sum_{j=1}^{n} f_j \ln[f_j]\right)$$

$$\text{subject to } \phi_i = \sum_{j=1}^{N} w_{ij} f_j$$

and $f_j \geq 0$

The accuracy of the computed field data depends on the optimization technique used to solve for the object function. In the present work, the Lagrange multiplier technique has been used to impose the constraints. This converts the MENT procedure to a relaxation scheme for solving a system of non-linear equations with the Lagrange multipliers as unknowns. The Gauss–Siedel method has been found to be adequate to solve for the unknowns. As in other algorithms, the three-dimensional field has been reconstructed plane-by-plane.

Minimum energy

The MENT algorithm can be generalized as an extremization of any functional $F(x,y,z)$ related to the field function $f(x,y,z)$. Gull and Newton[5] have suggested four such functions which can be extremized to solve the problem of reconstruction. Entropy and energy functions are attractive and natural in engineering. The minimum energy method as implemented is described below:

$$\text{maximize}\left(-\sum_{j=1}^{n} f_j^2\right)$$

$$\text{subject to } \phi_i = \sum_{j=1}^{n} w_{ij} f_j$$

Compared to MENT, the energy minimization is simple to formulate. However, Gull and Newton[5] have concluded that this method produces a field which is negatively correlated and hence biased.

Model object

The algorithms presented above have been tested with a phantom object that is generated using the equation[2]

$$\begin{aligned}\text{cosGauss}(x,y) = 1.09[&0.3\cos(x,y)\\ &+0.8(e^{\{-[9(x-0.2)]^2-[6(y-0.1)]^2\}}\\ &+e^{\{-[8(x+0.2)]^2-[6(y+0.35)]^2\}})]\end{aligned}$$

where

$$\begin{aligned}\cos(x,y) = 0.25&\{1-\cos[2\pi(x+0.5)^{4/5}]\}\\ &\times\{1-\cos[2\pi(y+0.5)^{4/5}]\}\end{aligned}$$

A numerically generated view of the phantom is shown in Figure 2.

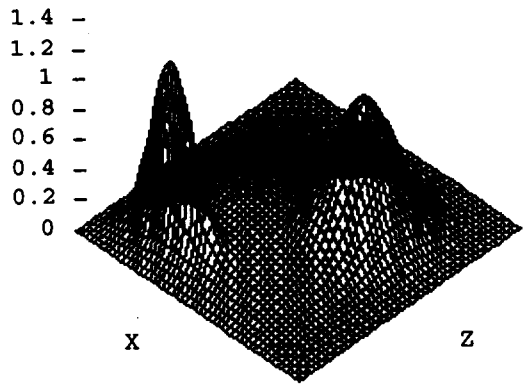

Figure 2 Schematic of the cosGauss phantom object

Table 1 Phantom object: performance of ART

Algorithm	Absolute max. error	RMS error (%)	CPU time (s)	No. of iterations
Simple ART	0.632	8.00	408.61	5001
Gordon ART	0.790	10.78	105.90	3379
Gilbert ART	0.634	8.00	191.84	5001
Anderson ART	0.634	8.00	216.08	5001

Table 2 Errors and convergence rates of simple ART

No. of projections	Total no. of rays	Angle of view	Absolute max. error	RMS error (%)	Time (s)	No. of iterations
2	100	90	0.852	13.18	0.88	53
3	199	90	0.687	9.01	2.34	118
5	496	90	0.632	8.00	408.61	5001
10	1383	90	0.350	5.11	1529.78	5001
5	418	180	0.583	7.22	4.26	118
9	932	180	0.466	6.25	263.18	3001
19	2726	180	0.143	3.38	312.74	2001

Table 3 Phantom object: performance of MART

	5 Projections, 418 rays and 180° view angle			
Algorithm	Absolute max. error	RMS error (%)	CPU time (s)	No. of iterations
MART 1	0.238	2.70	10.57	288
MART 2	0.238	2.70	8.44	187
MART 3	0.238	2.70	6.71	115

Table 4 Errors and convergence rates of MART3

No. of projections	Total no. of rays	Angle of view	Absolute max. error	RMS error (%)	Time (s)	No. of iterations
2	100	90	0.783	11.37	1.93	86
3	199	90	0.338	3.85	3.48	101
5	496	90	0.230	2.69	183.89	3001
10	1383	90	0.106	1.76	686.49	1602
5	418	180	0.238	2.70	6.71	115
9	932	180	0.141	1.70	121.43	597
10	1383	180	0.074	1.17	271.80	855
19	2726	180	0.031	0.48	574.01	712

Table 5 Phantom object: performance of MENT

No. of projections	No. of rays	Angle of view	Absolute max. error	RMS error (%)	Time (s)	No. of iterations
Maximum entropy: $\lambda = 0.05$						
2	100	90	0.784	11.37	0.84	108
3	199	90	0.342	3.87	4.19	114
5	496	90	0.362	3.82	61.51	238
10	1383	90	0.168	2.88	1451.23	622
5	418	180	0.238	2.70	17.11	168
9	932	180	0.348	3.22	90.95	1000

Table 6 Phantom object: performance of minimum energy

No. of projections	No. of rays	Angle of view	Absolute max. error	RMS error (%)	Time (s)	No. of iterations
Maximum energy: $\lambda = 1.0$						
2	100	90	0.952	14.06	0.41	20
3	119	90	0.744	10.02	0.82	46
5	496	90	0.738	9.77	4.91	59

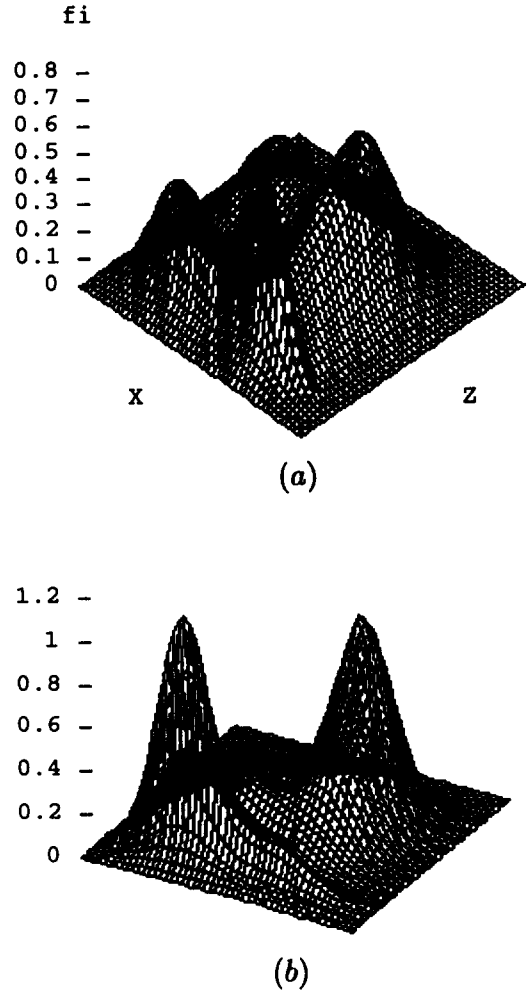

Figure 3 A cosGauss phantom object: (a) reconstructed data using two views, 0 and 90°; (b) reconstructed data using nine views, 0–180°

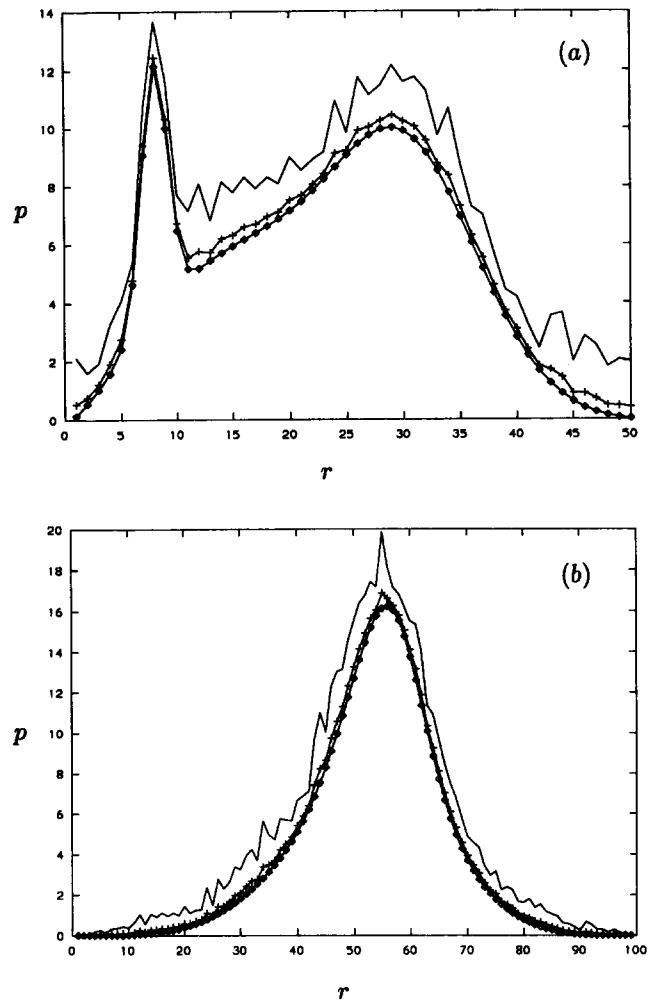

Figure 4 Projections of a cosGauss phantom object: (a) 0° projections, (b) 45° projections. -■-, noise level 0%; - + -, noise level 1%; ————, noise level 5%

Numerical data

In the present work, the object field is discretized into 50 × 50 cells of equal size. Assuming M_θ uniformly spaced rays and N_θ views, the total number of algebraic equations ($\Sigma_1^{N_\theta} M_\theta$) is typically 413 for five views. These equations are used to reproduce values of absorption coefficient at 2500 locations.

All algorithms considered here are iterative and a stopping criterion of 0.01% has been uniformly used. At convergence, the reconstructed and the original fields are separated by an amount, called error. Two error measures, namely

$$E_1 = \left| f(x,y,z) - \tilde{f}(x,y,z) \right|$$

and the normalized rms error

$$E_2 = \frac{\left\{ \dfrac{\sum_{j=1}^{N} \left[f(x,y,z) - \tilde{f}(x,y,z) \right]^2}{N} \right\}^{1/2}}{f(x,y,z)} \times 100$$

have been calculated in this study. Numerical computations

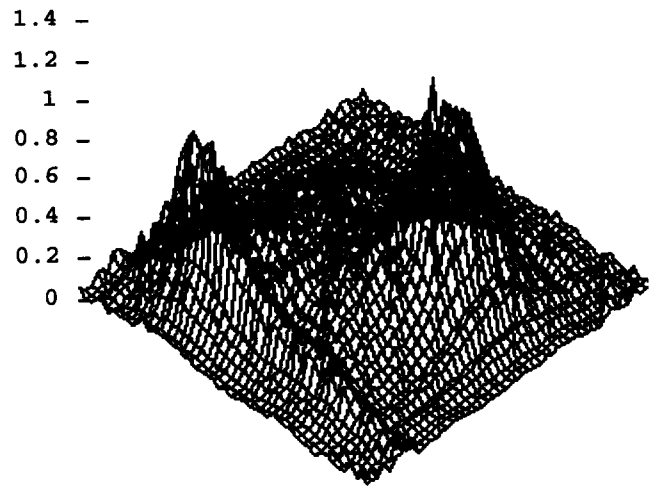

Figure 5 Reconstructed phantom using noisy data

were carried out on a DEC 3000/400 workstation with 32 MB RAM and a 175 MHz processor in single precision arithmetic.

Results

Results have been presented here for the reconstruction

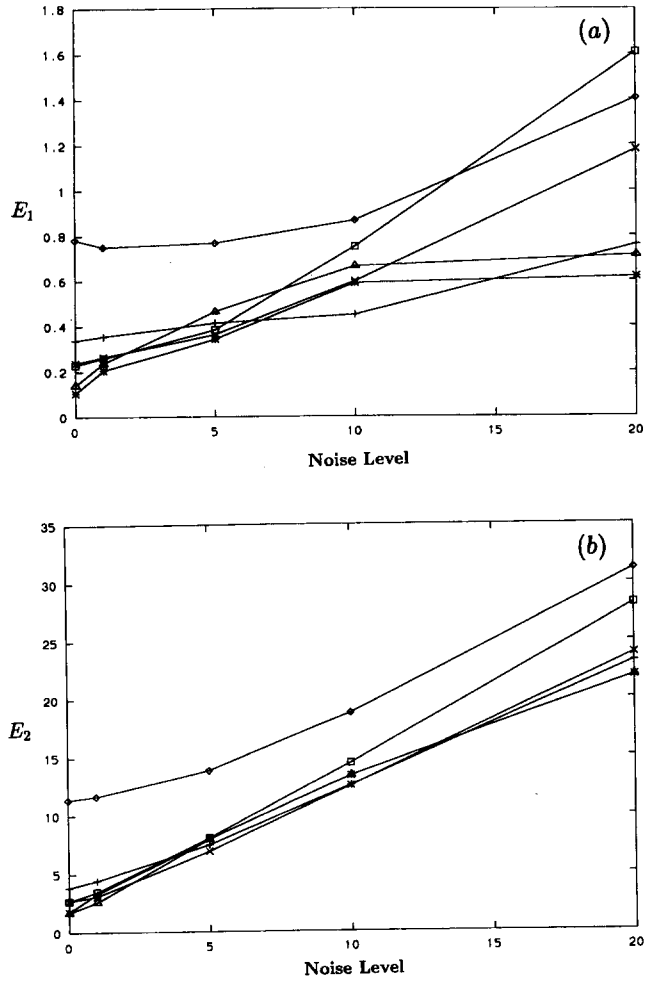

Figure 6 Variation of error levels with noise, MART3: (a) maximum absolute error E_1, (b) RMS error E_2. ♦, 2 projections; +, 3 projections; □, 5 projections (90); ×, 5 projections (180°); ▲, 9 projections; *, 10 projections

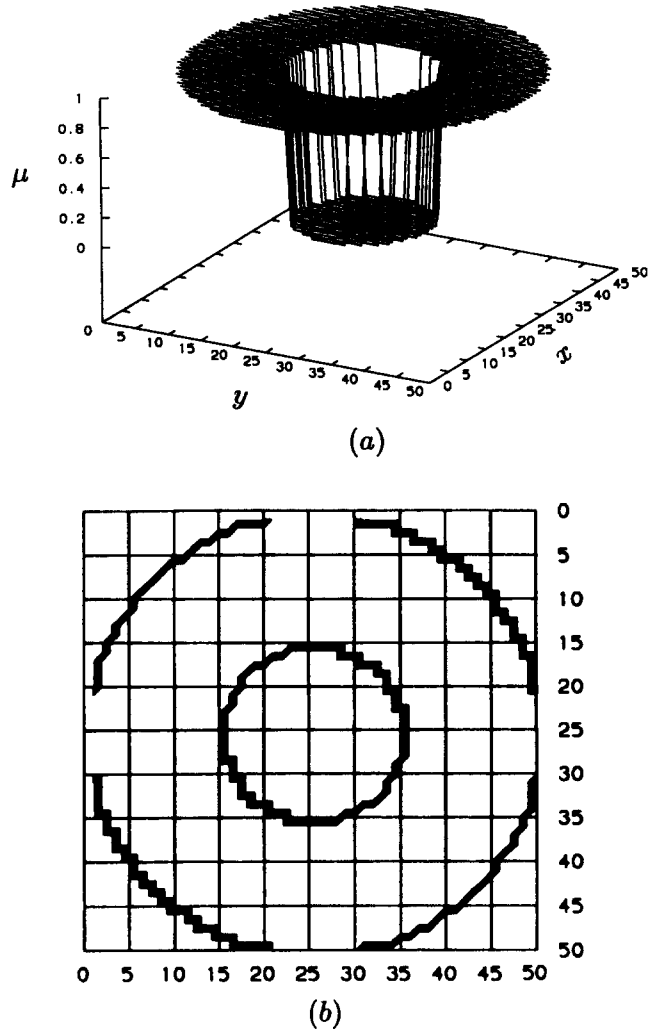

Figure 7 Circular plate with a circular hole: (a) distribution of original field μ; (b) contours of original field μ

algorithms described above, in terms of errors E_1 and E_2, number of iterations and sensitivity to noise in projection data.

Reconstruction errors

Errors due to reconstruction are examined here. The ART, MART and MENT group of algorithms are separately considered. A given algorithm works well within a range of relaxation parameters. The best value of the relaxation parameter which gives minimum error and fastest decay of error has been determined through numerical experiments and has been reported for each algorithm.

Errors in ART

Table 1 compares the performance of the ART family of algorithms. Simple ART reconstructs the field with lowest RMS as well as maximum absolute error. The error in the field predicted by Gilbert ART and Anderson ART are close to each other. Gordon ART has the largest maximum and RMS errors, but requires fewer iterations and a smaller CPU time. Simple ART is seen to require the largest number of iterations and the greatest CPU time. In the present work, simple ART is used for further analysis because of its simplicity and relatively better accuracy.

Simple ART is further analyzed by varying the number of projections, number of rays, noise level and angle of view. Table 2 is a summary of results obtained in this context at zero noise level. It can be seen that ART displays a systematic behaviour. An increase in the number of rays for a given total angle of view decreases the maximum and RMS errors. The location of the maximum error coincides with the jump surface in the field variable. Further, results predicted by three projections with a 90° view angle and five projections with a 180° view angle show that the errors are less in the latter. Similar results are seen in 10(90°)–10(180°) and 5(90°)–9(180°) projection sets. This shows that increasing the angle of view decreases the error levels. Errors also depend on the combination of projection angles. Numerical experiments show that meaningful results are obtained when at least two projections are orthogonal to each other.

Errors in MART

As described earlier, three forms of MART have been implemented. The largest relaxation factor that avoids

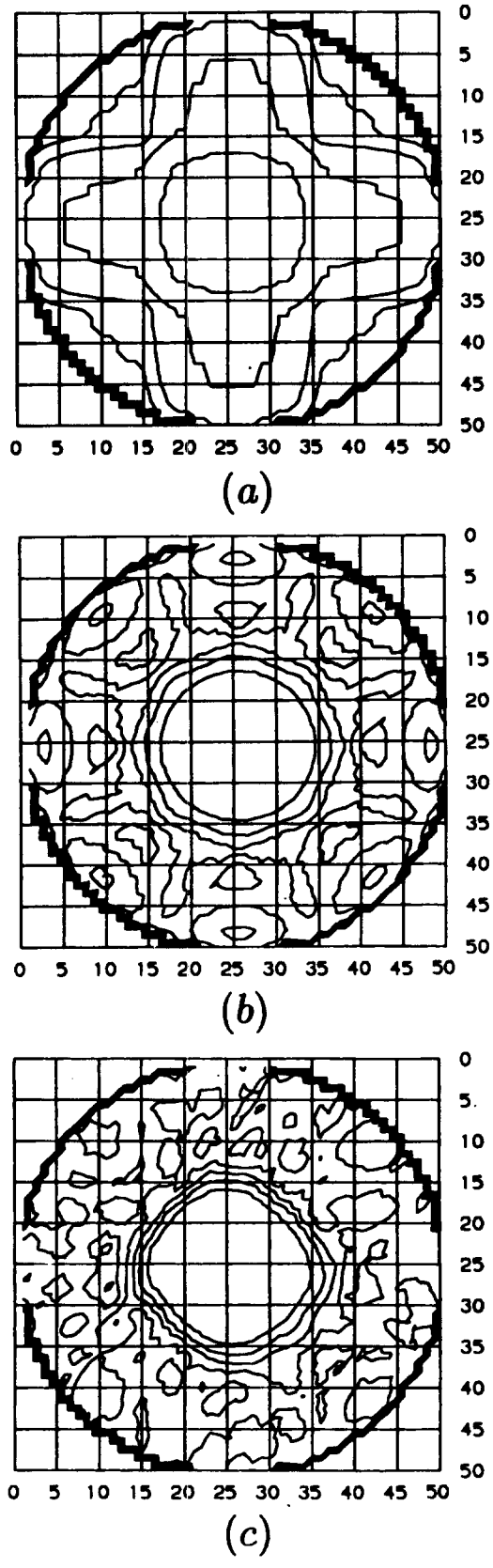

Figure 8 Circulate plate with a circular hole: contours of reconstructed field. (a) number of projections = 2 and angle of view = 90°; (b) number of projections = 5 and angle of view = 180°; (c) number of projections = 9 and angle of view = 180°

divergence has been used for computation. The three MART algorithms thus require different values of λ. The error estimates computed using 5(180°) projections for three forms of MART algorithms are given in Table 3. All the algorithms predict the shape of the phantom object with comparable error. However, convergence with MART3 is rapid and works with a high value of relaxation parameter. The overall error levels are much smaller than in ART algorithms. Table 4 shows the detailed performance MART3 with respect to the number of projections and angle of view. Error levels with a smaller number of views is high and these decay fast with increasing number of views.

A qualitative feel for the reconstructed object can be seen in Figure 3. Figure 3(a) and 3(b) show the reconstructed fields of the phantom that use two and nine projections, respectively. There are significant structural differences between Figures 2 and 3(a) while Figures 2 and 3(b) are quite similar.

Errors in MENT

Although MENT is an optimization-type of algorithm, MART converges to the MENT solution[3]. However, MENT reduces the problem of reconstruction to a solution of non-linear simultaneous equations which can be solved by a Gauss–Siedel iteration scheme. Table 5 shows the error levels observed using MENT. When the number of projections is high, the error levels in MENT are seen to be high when compared to MART. However the overall characteristics of convergence are similar to MART.

The minimum energy method (Section 3.6) has also been tested using two to five projections. It converges rapidly but its performance is poor and error levels are high (Table 6).

Effect of noise levels on reconstruction errors

The performance of the algorithms given above has been determined using perfect (projection) data. An overall conclusion that can be drawn is that MART3 is better when compared to the other algorithms. In experiments, the projection data will be superimposed with noise. Since the reconstruction algorithms address inversion of ill-conditioned matrices, it is reasonable to expect each of them to be sensitive to noise in the data. In the present study, the issue of amplification of noise during reconstruction is addressed. For definiteness, MART3 is used to invert the noisy data.

Noise in data comes from various sources, such as the method of the experimental technique and types of source and detector. For example, for a γ-ray source the initial intensity I_0 has a Poisson distribution in time. This introduces noise in the projections and this will also have a Poisson distribution since the projection operator (the path integral) is linear. In the present work, noise (up to 20%) using a Poisson random number generator has been added to projection data. Figure 4(a) and 4(b) compare the 0–45° projections of the phantom object with 0, 1 and 5% noise levels. Errors in reconstruction have been determined consistently with respect to the original model (noise-free) object.

Figure 5 shows a reconstructed phantom using noisy data.

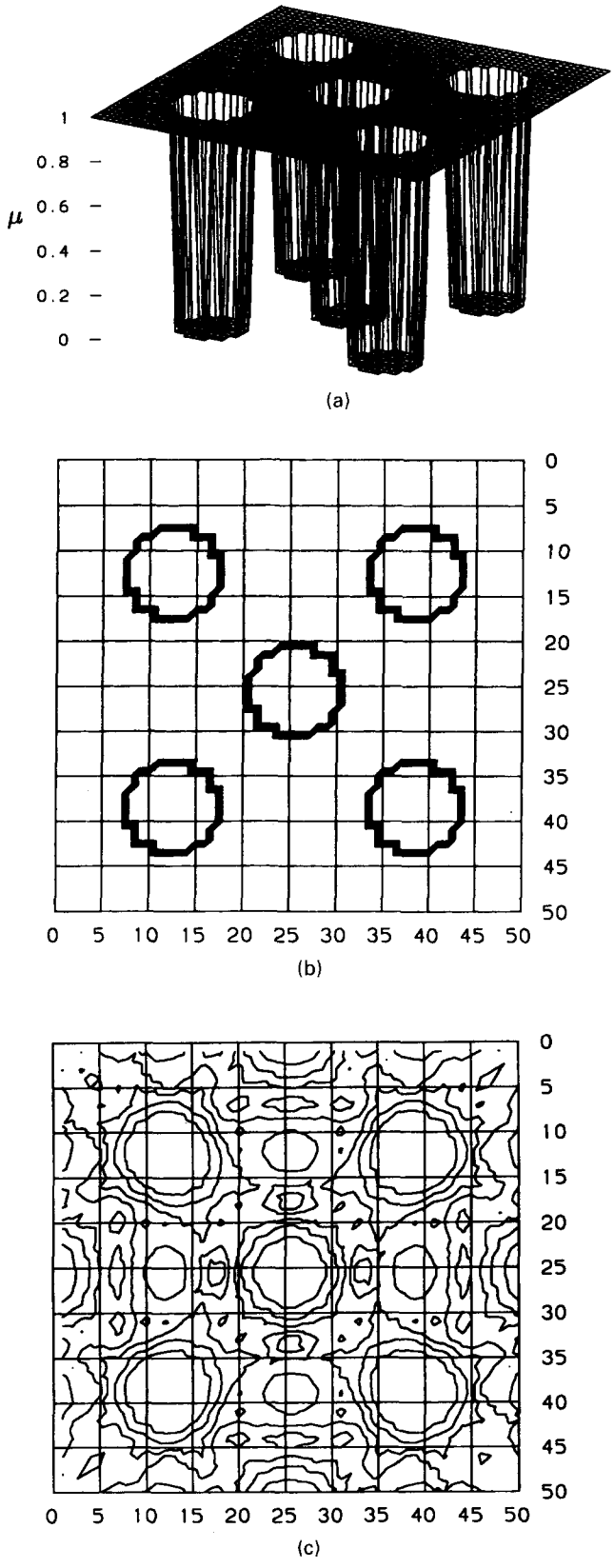

Figure 9 Square plate with five circular holes: (a) distribution of original field μ; (b) contours of original field μ; (c) contours of reconstructed field μ

At 5% noise, the reconstructed image is clearly recognizable in terms of peaks and valleys. Figure 6 shows the extent of reconstruction errors in MART3 as a function of noise in the projection data. Several combinations of views and projection angles have been considered. The results shown

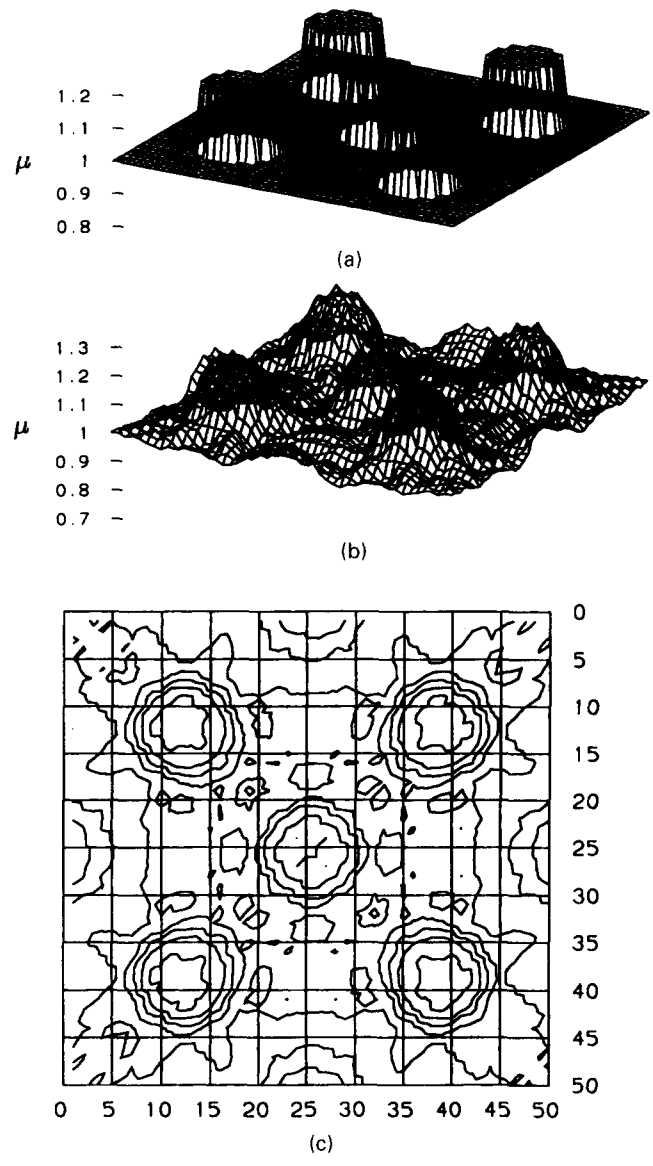

Figure 10 Square plate with five circular inclusions: (a) distribution of original field μ; (b) distribution of reconstructed field μ; (c) contours of reconstructed field μ

increase in error (E_1 as well as E_2) with noise in the input data. The RMS error in reconstruction is consistently larger than the noise level in the projections, varying by a factor of 1.1–2. A large number of views with a limited projection angle (10 and 90°, for example) in fact leads to deterioration of errors from the projections. While no clear trend is seen in the maximum error, the RMS error shows the following result. Fewer views with a larger view angle amplify noise in the input data to a minimum extent. In contrast, a greater number of views and a smaller view angle amplify noise significantly.

The algorithms presented above are now used to reconstruct physical objects with internal features.

Application 1: circular plate with a central hole

A circular plate with a circular hole is simulated as an object with an absorption coefficient of 1 everywhere outside the

hole and 0 inside the hole. Figure 7(a) shows the discretized object field for the circular plate and Figure 7(b) shows the contours of Figure 7(a). The circular plate with 50 units diameter has a hole of 20 units. Numerical integration is carried out to generate projections. MART3 with 2(90°), 5(180°) and 9(180°) projections is used to reconstruct the object. Figure 8 shows the reconstructed contours of the absorption coefficient using two, five and nine projections.

Figure 8(a) shows the absorption coefficient of the plate reconstructed using two projections. It shows many contours of the absorption coefficient, the innermost contour having a value of 0.244. The value of the absorption coefficient is much higher outside this contour and lower than 0.244 inside. Therefore, this contour can be assumed to be the edge of the circle. The original circular hole is predicted as a square hole with rounded corners. Figure 8(b) shows the reconstructed object using five projections. The innermost contour whose value is 0.220 has a circular shape. However its size is less than the actual size of the hole. Finally, Figure 8(c) (with nine projections) shows a contour which is nearly circular in shape and is close to the actual size of the hole.

Application 2: square plate with five holes

The object studied in Application 1 is simple in shape. General industrial objects will have complex geometries and a greater number of voids and inclusions. Figure 9(a) and 9(b) shows the simulation of field data for square plate with five holes. The plate is square of 50 × 50 units and has five holes, each having a radius of 5 units. The field is represented as an absorption coefficient equal to 1 everywhere outside the holes and 0 inside the holes. Figure 9(c) shows the contours of the absorption coefficient in the reconstructed field using MART3 with five projections. Five small, nearly circular, contours with an identical value of 0.225 are seen in this figure.

Application 3: square plate with five circular inclusions

In Applications 1 and 2, the field has a value of 0 and 1 which clearly distinguishes the holes from the objects. In this section circular holes are replaced by circular inclusions whose absorption coefficient is slightly larger than the plate material. Figure 10(a) shows the distribution of field value; a value of 1 is given outside the inclusions and 1.2 within the inclusions. Figure 10(b) shows the reconstructed field using MART3 and Figure 10(c) shows the contours of reconstructed field. Five circular regions are clearly seen in the figure. The innermost circular contours have a field value of 1.19, while it is less than 1.1 outside these contours. Hence the algorithms are seen to predict the presence of inclusions in the plate.

Conclusions

The performance of ART, MART and MENT family of algorithms under limited data conditions (when applied to simulated objects in NDT) is presented. The major observations of the study are as follows.

- MART3 performs better than all other algorithms.
- All algorithms considered show a systematic behaviour with respect to the number of projections, view angle and noise level.
- Simple ART accommodates with a high value of relaxation. However, its performance is poor when compared to MART.
- The minimum energy method predicts a field with high error.
- Noise amplification is reduced for all algorithms if fewer views and a large view angle are considered.
- The size and shape of the voids and inclusions (present inside solid objects) are predicted reasonably well.

Nomenclature

dx, dz	cell sizes respectively in the x and z directions
e	stopping criterion
E_1	absolute maximum error
E_2	RMS value of error
f_j	field value of the jth cell
f_j^2	energy of field f_j
F_j	entropy of field f_j
I_0	Initial intensity of the radiation at the entrance
$I(r,\theta)$	intensity of the radiation at the exit
l_{ij}	length of intercept
M	grand total number of rays
M_θ	total number of rays per view
N	total number of cells
r	coordinate normal to the direction of irradiation
s	path along measuring beam
w_{ij}	weight function
x, y, z	Cartesian coordinates
X, Y, S	Fourier wavenumber

Greek letters

$\phi_{i\theta}$	projection due to the i_θth ray
$\Delta\phi_{i\theta}$	correction due to the i_θth ray
λ	relaxation parameter
μ	absorption coefficient

References

1 **Gordon, R., Bender, R. and Herman, G.T.,** Algebraic reconstruction techniques (ART) for three-dimensional electron microscopy and X-ray photography. *J. Theor. Biol.*, 1970, **29**, 471–481.

2 **Verhoeven, D.,** Multiplicative algebraic computed tomographic algorithms for the reconstruction of multidirectional interferometric data. *Opt. Eng.* , 1993, **32**, 410–419.

3 **Minerbo, G.,** MENT: a maximum entropy algorithm for reconstructing a source from projection data. *Computer Graphics Image Processing*, 1979, **10**, 48–68.

4 **Censor, Y.,** Finite series-expansion reconstruction methods. *Proc. IEEE*, 1983, **71**, 409–419.

5 **Gull, S.F. and Newton, T.J.,** Maximum entropy tomography. *Appl. Opt.* , 1986, **25**, 156–160.

6 **Herman, G.T.,** Mathematical optimization versus practical performance: a case study based on the maximum entropy criterion in image reconstruction. *Math. Prog. Study*, 1981, **20**, 96–112.

7 **Myers, K.J. and Hanson, K.M.,** Comparison of the algebraic reconstruction technique with maximum entropy reconstruction technique for a variety of detection tasks. *Medical Imaging IV: Image Formation*, 1990, **1231**, 176–186.

8 **Reis, M.L. and Roberty, N.C.,** Maximum entropy algorithms for image reconstruction from projections. *Inverse Problems*, 1992, **8**, 623–644.

9 **Natterer, F.,** *The Mathematics of Computerized Tomography*, Wiley, Chichester, UK, 1986.

10 **Bracewell, R.N.,** Strip integration in radio astronomy. *Aust. J. Phys.* , 1965, **9**, 198–217.

11 **Herman, G.T.,** *Image from Projections*, Academic Press, New York, 1980.

12 **Munshi, P.,** Error analysis of tomographic filters I: theory. *NDT & E. Int.*, 1992, **25**, 191-194.

13 **Subbarao, P.M.V. and Muralidhar, K.,** Noise removal, three dimensional reconstruction and data retrieval for optical images of stratified fluids, Report, Department of Science and Technology, Government of India, 1996.

14 **Mayinger, F.,** *Optical Measurements*, Springer–Verlag, New York, 1994.

15 **Gilbert, P.F.C.,** Iterative methods for three-dimensional reconstruction of an object from its projections. *J. Theo. Biol.*, 1972, **36**, 105–117.

16 **Anderson, A.H. and Kak, A.C.,** Simultaneous algebraic reconstruction technique (SART): a superior implementation of the ART algorithm. *Ultrason. Imaging*, 1984, **6**.